NANO LETTERS
pubs.acs.org/NanoLett Letter

Even–Odd Layer-Dependent Exchange Bias Effect in $MnBi_2Te_4$ Chern Insulator Devices

Bo Chen,[$] Xiaoda Liu,[$] Yuhang Li,[$] Han Tay, Takashi Taniguchi, Kenji Watanabe, Moses H. W. Chan, Jiaqiang Yan, Fengqi Song, Ran Cheng,* and Cui-Zu Chang*

Cite This: Nano Lett. 2024, 24, 8320–8326 Read Online

ACCESS | Metrics & More | Article Recommendations | Supporting Information

ABSTRACT: Magnetic topological materials with coexisting magnetism and nontrivial band structures exhibit many novel quantum phenomena, including the quantum anomalous Hall effect, the axion insulator state, and the Weyl semimetal phase. As a stoichiometric layered antiferromagnetic topological insulator, thin films of $MnBi_2Te_4$ show fascinating even–odd layer-dependent physics. In this work, we fabricate a series of thin-flake $MnBi_2Te_4$ devices using stencil masks and observe the Chern insulator state at high magnetic fields. Upon magnetic field training, a large exchange bias effect is observed in odd but not in even septuple layer (SL) devices. Through theoretical calculations, we attribute the even–odd layer-dependent exchange bias effect to the contrasting surface and bulk magnetic properties of $MnBi_2Te_4$ devices. Our findings reveal the microscopic magnetic configuration of $MnBi_2Te_4$ thin flakes and highlight the challenges in replicating the zero magnetic field quantum anomalous Hall effect in odd SL $MnBi_2Te_4$ devices.

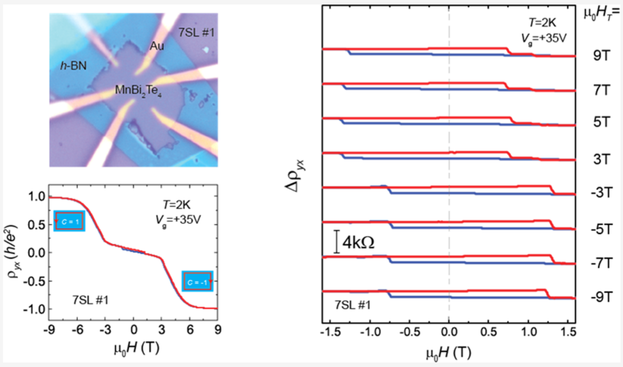

KEYWORDS: *intrinsic magnetic topological insulator, Chern insulator, exchange bias effect, antiferromagnetism, stencil mask*

Over the last one and a half decades, the interplay between band topology and magnetism has been a major driving force underlying the discovery of a new class of materials known as magnetic topological materials.[1−9] These materials not only host boundary electronic states carrying dissipationless currents but also exhibit a novel magnetoelectric behavior known as "axion electrodynamics".[9] As a consequence, magnetic topological materials are of great importance in both fundamental science and practical applications. Newly discovered magnetic topological states include but are not limited to the quantum anomalous Hall (QAH) state,[4,9−13] the axion insulator state,[14−16] the magnetic Weyl semimetal phase,[17,18] and the high-order magnetic topological insulator (TI) state.[19,20] Traditional ways of entangling band topology with magnetism typically involve either introducing magnetic ions into TI materials or fabricating TI/ferromagnet heterostructures,[6,21] but the magnetic topological materials opened an ideal platform where a single crystalline material can host coexisting topological and magnetic states intrinsically.

$MnBi_2Te_4$, a stoichiometric tetradymite-type antiferromagnetic (AFM) semiconductor, is an intrinsic magnetic TI (refs 9 and 22−26). The lattice structure of $MnBi_2Te_4$ can be viewed as intercalating a MnTe bilayer into a Bi_2Te_3 quintuple layer, forming a septuple layer (SL) structure (Figure 1a). The magnetic properties of $MnBi_2Te_4$ originate from the Mn 3d local moments. The Mn^{2+} ions are located at SL centers and carry 5 μ_B magnetic moments (μ_B represents the Bohr magneton). While the intra-SL exchange interaction is ferromagnetic, the inter-SL exchange interaction is AFM, which leads to an A-type (i.e., layered) AFM order. The Néel temperature T_N of $MnBi_2Te_4$ bulk crystals is ~25 K. This layered AFM order in $MnBi_2Te_4$ thin films usually gives rise to even–odd SL-dependent physics,[9,22−25,27] as the magnetic moments in the top and bottom surfaces are parallel-(antiparallel) in a sample with odd (even) SLs. Correspondingly, the total Hall conductance is 0 in even SLs (i.e., the axion insulator state) and e^2/h in odd SLs (i.e., the QAH state) under zero magnetic field.[22,23,27] Experimental efforts along this direction include the observations of the zero magnetic field QAH effect in a 5 SL $MnBi_2Te_4$ device[13] and the axion insulator state in 6 SL devices.[28] However, over the last five years, the replication of this zero magnetic field QAH state remains difficult. Nonetheless, the Chern insulator state under high magnetic fields has been repeatedly observed in both even- and odd-SL $MnBi_2Te_4$ devices when the magnetic

Received: April 3, 2024
Revised: June 25, 2024
Accepted: June 26, 2024
Published: June 27, 2024

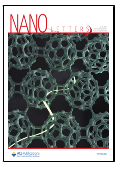

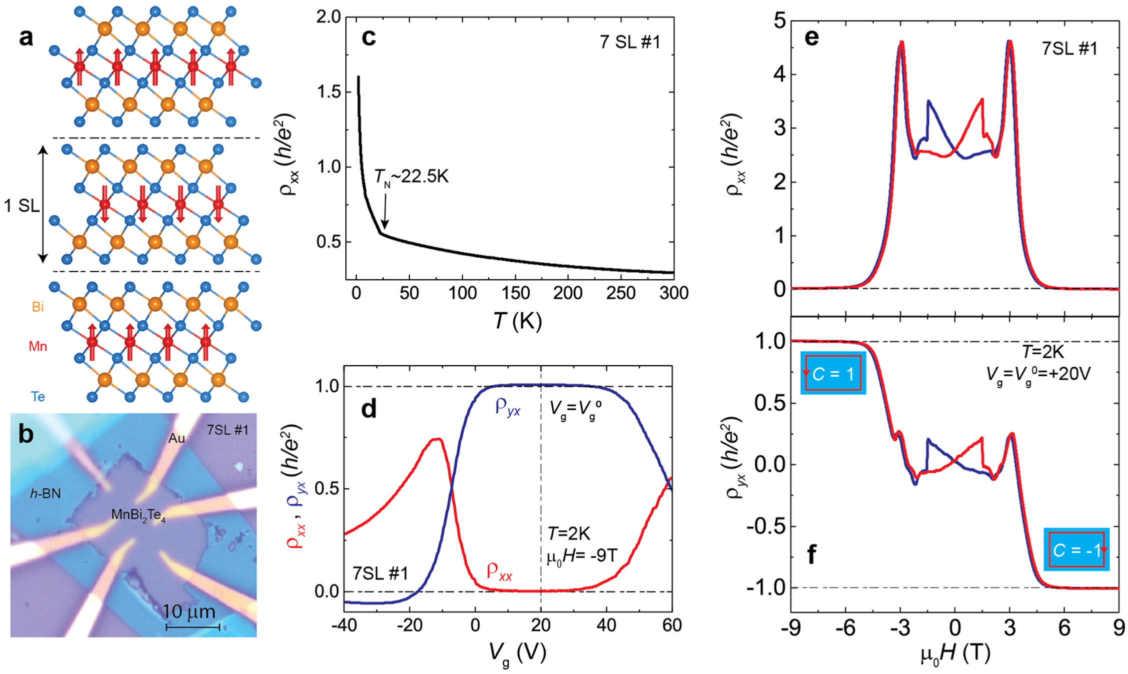

Figure 1. The Chern insulator state in a 7 SL $MnBi_2Te_4$ device (7SL #1). (a) Crystal structure of $MnBi_2Te_4$. The red arrows indicate the magnetic moment of the Mn layers. (b) Optical image of Device 7SL #1. (c) Temperature dependence of ρ_{xx} at V_g = 0 V. (d) V_g dependence of ρ_{yx} (blue) and ρ_{xx} (red) at $\mu_0 H = -9$ T and $T = 2$ K. (e, f) $\mu_0 H$ dependence of ρ_{xx} (e) and ρ_{yx} (f) at $V_g = V_g^0$ = +20 V and T = 2 K. The charge neutral point V_g^0 is determined as the voltage at which ρ_{xx} reaches its minimum value.

moments of Mn^{2+} ions are aligned in the same direction (i.e., ferromagnetic state).[28−34] Therefore, an SL-resolved and microscopic magnetic configuration of $MnBi_2Te_4$ thin flakes near zero magnetic field is not yet fully understood.

The exchange bias effect, which is commonly observed in ferromagnet/antiferromagnet bilayers has been used to reveal the microscopic configuration of magnetic materials.[35,36] The AFM layer typically serves as a pinning layer whose ordering direction determines the shift direction of the hysteresis loop in the ferromagnetic layer. By employing either magnetic field cooling (MFC) or magnetic field training (MFT) procedures, the hysteresis loop shift of the ferromagnetic layer can provide insights into the microscopic magnetic configuration across the interface.[37−40] Recently, the exchange bias effect has been observed in both $MnBi_2Te_4/Cr_2Ge_2Te_6$ and $MnBi_2Te_4/CrI_3$ heterostructures (refs 41−43). Moreover, reflective magnetic circular dichroism (RMCD) measurements also revealed the exchange bias effect in ferromagnetic $MnSb_2Te_4$ down to one SL and thin flakes of $MnBi_4Te_7$ and $MnBi_6Te_{10}$, even in the absence of the ferromagnetic capping layers.[44,45] The observation of the exchange bias effect in these samples has been attributed to the formation of magnetic domains induced by Mn/(Bi, Sb) antisites.[44,45] To date, none of the $MnBi_2Te_4$ devices with well-quantized Chern insulator states[9,13,28−34] show the exchange bias effect.

In this work, we fabricate a series of $MnBi_2Te_4$ devices with thicknesses varying from 5 to 8 SL. All these $MnBi_2Te_4$ devices exhibit the Chern insulator state under high magnetic fields. Through electrical transport measurements, we observe a square hysteresis loop near zero magnetic field in all these devices. Upon magnetic field training, a large negative exchange bias effect is observed in the odd but not in the even SL devices. This observation indicates that an uncompensated AFM ground state is essential for the appearance of the exchange bias effect in $MnBi_2Te_4$. Through a detailed theoretical analysis, we attribute the SL-dependent exchange bias effect to the different surface and bulk magnetic properties of the SLs. The observed SL-dependent exchange bias effect sheds significant light on the microscopic magnetic configuration in $MnBi_2Te_4$ thin films.

All of the $MnBi_2Te_4$ devices are fabricated on silicon wafers that are coated with 285 nm of SiO_2. The gold contacts are deposited using a SiN_x stencil mask, avoiding contamination from solvents throughout the lithography process. Subsequently, a thin h-BN flake is applied to cap the $MnBi_2Te_4$ device to protect it from degradation during exposure to air. The thicknesses of $MnBi_2Te_4$ thin flakes are determined through their optical contrast and atomic force microscopy measurements (Supplementary Figure 1).[13,33] The electrical transport studies are conducted in a Physical Property Measurement System cryostat (Quantum Design DynaCool, 1.7 K, 9 T). All transport measurements are performed by a standard lock-in technique with an excitation current of 10−200 nA. More details about the device fabrication and electrical transport measurements can be found in the Supporting Information.

We first focus on the demonstration of the Chern insulator state under high magnetic fields in a 7 SL $MnBi_2Te_4$ device (denoted as 7SL #1). Figure 1b shows the optical image of 7SL #1, which is covered by a thin h-BN flake. Next, we perform electrical transport measurements on 7SL #1 and observe that its longitudinal resistance ρ_{xx} increases monotonically with decreasing temperature (Figure 1c), confirming the existence of an insulating ground state. A sudden upturn appears at $T \sim$ 22.5 K, locating the T_N value of 7SL #1. Figure 1d shows the bottom gate V_g dependence of ρ_{xx} and Hall resistance ρ_{yx} measured at magnetic field $\mu_0 H = -9$ T and $T = 2$ K. For +5 V $\leq V_g \leq$ +35 V, a wide quantized ρ_{yx} plateau and vanishing ρ_{xx} are observed. This observation validates the existence of the Chern insulator state in 7SL #1, consistent with prior

https://doi.org/10.1021/acs.nanolett.4c01597
Nano Lett. 2024, 24, 8320−8326

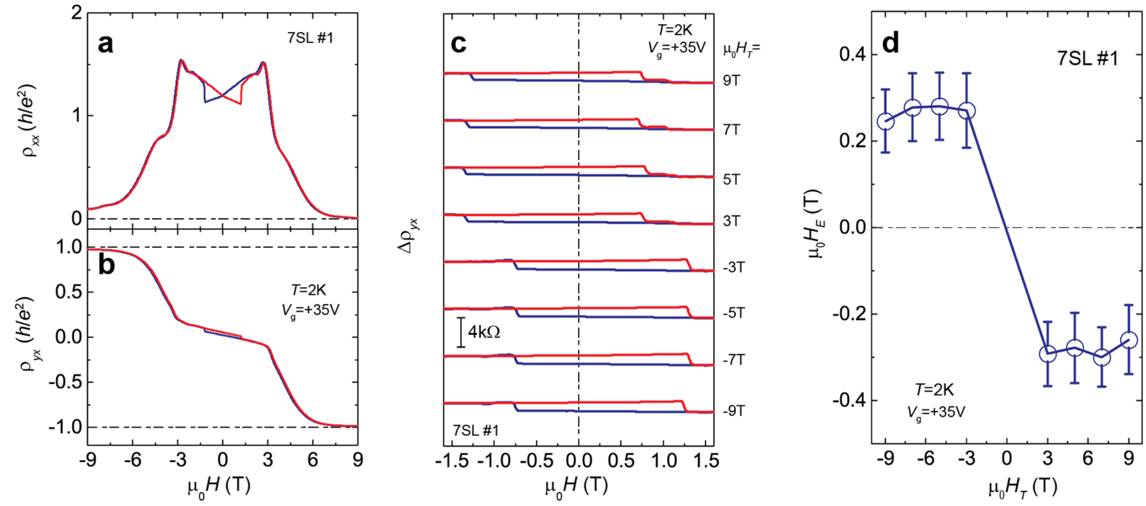

Figure 2. The negative exchange bias effect in the 7 SL $MnBi_2Te_4$ device (7SL #1). (a, b) μ_0H dependence of ρ_{xx} (a) and ρ_{yx} (b) at V_g = +35 V and T = 2 K. (c) The negative exchange bias effect under magnetic field training (MFT). The AH resistance $\Delta\rho_{yx}$ is shown by subtracting the linear background. (d) The value of the exchange bias field μ_0H_E as a function of the external training magnetic field μ_0H_T. The error bars in (d) are estimated from the transition widths near the coercive field μ_0H_c of the hysteresis in (c).

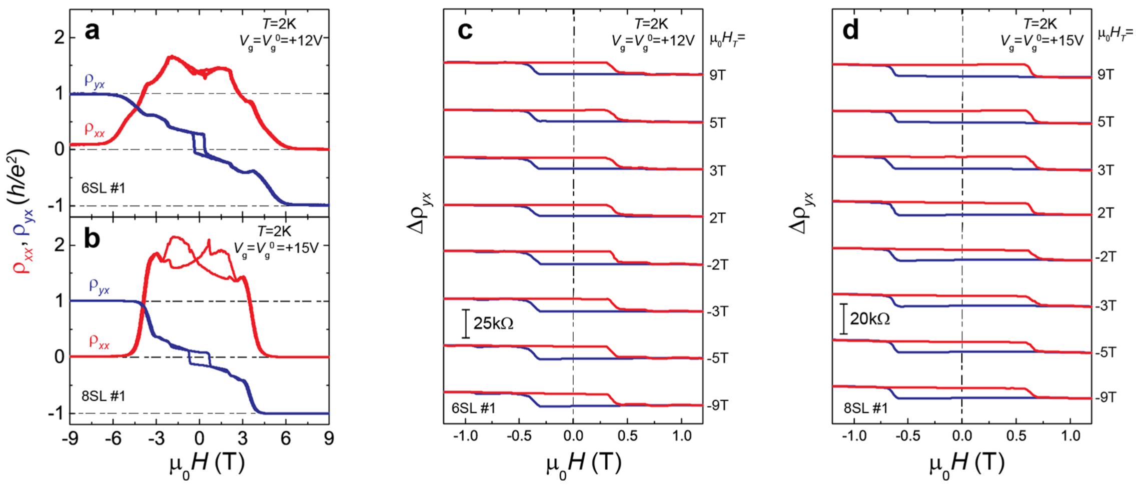

Figure 3. Absence of the exchange bias effect in 6 SL and 8 SL $MnBi_2Te_4$ devices (6SL #1 and 8SL #1). (a, b) μ_0H dependence of ρ_{xx} (red) and ρ_{yx}(blue) in 6 SL (a) and 8SL (b) $MnBi_2Te_4$ devices at $V_g = V_g^0$ and T = 2 K. Both devices exhibit the Chern insulator state under high μ_0H. (c, d) Absence of the exchange bias effect under MFT in 6 SL (c) and 8SL (d) $MnBi_2Te_4$ devices. For $\mu_0H_T \geq 2$ T, μ_0H sweeps from μ_0H_T to −1.2 T to +1.2 T. For $\mu_0H_T \leq -2$ T, μ_0H sweeps from μ_0H_T to +1.2 T to −1.2 T. $\Delta\rho_{yx}$ in (c) and (d) are shown by subtracting the linear background.

studies.[13,28−30] We define the value of the charge neutral point V_g^0 as the midpoint of the quantized ρ_{yx} plateau. At $V_g = V_g^0$ = +20 V, ρ_{yx} is quantized at $\sim h/e^2$ for $\mu_0H \geq 5$ T, concomitant with vanishing ρ_{xx} (Figure 1e and f). This observation confirms the well-quantized Chern insulator state for $\mu_0H \geq 5$ T in 7SL #1.

Besides the Chern insulator state observed in the ferromagnetic regime, a butterfly feature is observed near zero magnetic field in both ρ_{xx} and ρ_{yx}, i.e., the AFM regime (Figure 1e and f). The butterfly kinks occur at $\mu_0H \sim \pm 1.48$ T, corresponding to the coercive field μ_0H_c of the magnetic hysteresis loop. The appearance of the butterfly feature instead of the square hysteresis loop in ρ_{yx} near zero magnetic field is probably due to the mutual pickup between ρ_{xx} and ρ_{yx}, as ρ_{xx} is significantly larger than ρ_{yx} in this regime (Figure 1f). To mitigate this pickup while maintaining the quantized ρ_{yx}, we measure the μ_0H dependence of ρ_{xx} and ρ_{yx} at V_g = +35 V (Figure 2). A square hysteresis loop is observed in ρ_{yx} near zero magnetic field, corresponding to a reversed butterfly feature in ρ_{xx} (Figure 2a and b). For $\mu_0H \geq 8$ T, ρ_{yx} is still nearly quantized. Therefore, the anomalous Hall hysteresis loop is observed in 7SL #1 near zero magnetic field when the sample exhibits the Chern insulator state under high magnetic fields (i.e., the ferromagnetic regime).

Next, we examine the anomalous Hall hysteresis loop near zero magnetic field in 7SL #1. By applying an external μ_0H, the AFM state in $MnBi_2Te_4$ can be driven to a canted AFM state [i.e., the spins of the adjacent septuple layers are no longer parallel (or antiparallel)] and ultimately to a ferromagnetic state (i.e., the spins of all septuple layers are parallel) (refs 30 and 46). The magnetic field at which the transition from the AFM state to the canted AFM state occurs is defined as the spin-flop magnetic field μ_0H_s. First, we cool down 7SL #1 to T = 2 K under zero magnetic field and subsequently apply a magnetic training field $|\mu_0H_T|$ exceeding $|\mu_0H_s| \sim 2.75$ T, specifically, $|\mu_0H_T| \geq 3$ T. Next, we sweep μ_0H from μ_0H_T to −1.6 T and then to +1.6 T for $\mu_0H_T > 0$. Conversely, for $\mu_0H_T < 0$, the μ_0H sweep is from μ_0H_T to +1.6 T and then back to

https://doi.org/10.1021/acs.nanolett.4c01597
Nano Lett. 2024, 24, 8320−8326

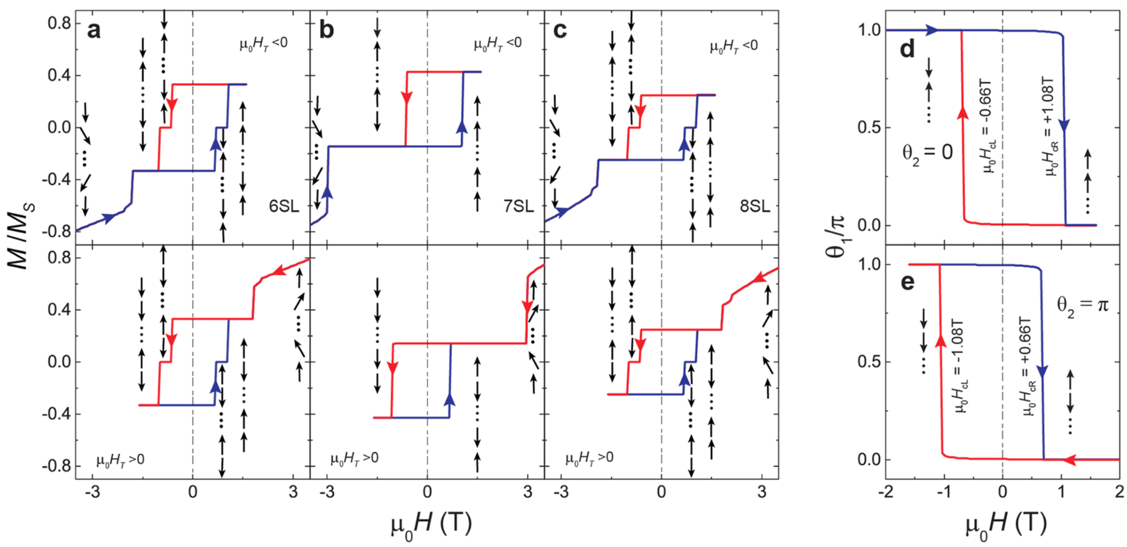

Figure 4. Simulation of the exchanged bias effect in even and odd SL $MnBi_2Te_4$ devices. (a−c) μ_0H dependence of the total magnetization M in $MnBi_2Te_4$ devices under $\mu_0H_T < 0$ (top) and $\mu_0H_T > 0$ (bottom). M_s is the saturated magnetization under high magnetic fields. Schematics of magnetic configurations at $\mu_0H = \pm0.9$, ±1.5, and ±3.1 T are plotted. (a) 6SL, (b) 7SL, (c) 8SL. (d, e) Evolution of the magnetic moment angle of the top SL (θ_1) under high MFT when the magnetization in the second top SL points upward ($\theta_2 = 0$, d) and downward ($\theta_2 = \pi$, e). The magnetic moment angle of the bottom SL (θ_N) shows similar behavior: $|\mu_0H_{cR}| > |\mu_0H_{cL}|$ ($|\mu_0H_{cR}| < |\mu_0H_{cL}|$) for $\theta_{N-1} = 0$ (π). The magnetization is obtained by minimizing the free energy. The values of μ_0H_{cR} and μ_0H_{cL} occur where one local minimum of the free energy near $\theta_1 = 0$ (π) disappears while the system jumps to another one near $\theta_1 = \pi(0)$.

−1.6 T. For $\mu_0H_T \geq 3$ T, the magnetic hysteresis loop shifts toward the negative magnetic field direction, while, for $\mu_0H_T \leq -3$ T, the magnetic hysteresis loop shifts toward the positive magnetic field direction (Figure 2c). This observation confirms the existence of the negative exchange bias effect in 7SL #1. We define the exchange bias field μ_0H_E as $(\mu_0H_{cR} - \mu_0H_{cL})/2$, where μ_0H_{cR} and μ_0H_{cL} represent the right and left coercive fields, respectively. The value of $|\mu_0H_E|$ is found to be ∼0.28 T with minimal variation for both $\mu_0H_T \geq 3$ T and $\mu_0H_T \leq -3$ T (Figure 2d).

Supplementary Figure 3 shows the exchange bias effect under different temperatures and gate voltages in 7SL #1. We find that for $\mu_0H_T = 3$ T the exchange bias effect becomes weaker with increasing temperatures and vanishes at $T = 15$ K (Supplementary Figure 3a). Note that the magnetic hysteresis loop disappears at $T = 25$ K, consistent with $T_N \sim 22.5$ K of 7SL #1 (Figure 1c). Moreover, by varying V_g from +50 V to −20 V, the carrier type of 7SL #1 is tuned from p- to n-type. Remarkably, the negative exchange bias effect persists at all of the V_gs. Even for $V_g = V_g^0$, the negative exchange bias effect is discernible through ρ_{xx} (Supplementary Figure 3b). The same phenomena are observed in both a 5 SL (5SL #1) device and an additional 7 SL (7SL #2) device (Supplementary Figures 4 and 5). The persistent occurrence of the negative exchange bias effect in all of these odd SL $MnBi_2Te_4$ devices points to an intrinsic mechanism associated with their microscopic magnetic configuration.

Unlike the odd SL $MnBi_2Te_4$ devices, the exchange bias effect is absent in even SL $MnBi_2Te_4$ devices (Figure 3). First, we demonstrate the Chern insulator state in both the 6 SL (6SL #1) and 8 SL (8SL #1) $MnBi_2Te_4$ devices. For 6SL #1, quantized ρ_{yx} and vanishing ρ_{xx} are observed for $\mu_0H \geq 6.5$ T (Figure 3a). However, for 8SL #1, these behaviors occur for $\mu_0H \geq 4.2$ T (Figure 3b). The much lower μ_0H required for the realization of the Chern insulator state in 8SL #1 is likely attributed to the high quality of the device, which can induce the Chern insulator state in its canted AFM regime.[31] For both 6SL #1 and 8SL #1, a magnetic hysteresis loop near zero magnetic field is also observed, consistent with prior studies.[30,31] The formation of the hysteresis loop in even SL $MnBi_2Te_4$ devices has been attributed to the presence of native magnetic disorders and/or surface asymmetry induced during the fabrication process.[30,31,46]

Next, we apply the same MFT process used for the odd SL devices to the even SL devices. For both 6SL #1 and 8SL #1, the value of $|\mu_0H_s|$ is ∼1.9 T, slightly smaller than that of 7SL #1 (refs 9, 30, and 46). As noted above, to create the initial magnetic state in a $MnBi_2Te_4$ device, we need to apply $|\mu_0H_T|$ greater than $|\mu_0H_s|$. Given that the values of $|\mu_0H_c|$ are ∼0.38 T for 6SL #1 and ∼0.64 T for 8SL#1, we sweep μ_0H from μ_0H_T to −1.2 T and then to +1.2 T for $\mu_0H_T > 0$ and from μ_0H_T to +1.2 T and then back to −1.2 T for $\mu_0H_T < 0$ (Figure 3c and d). We observe that, for $\mu_0H_T \geq 2$ T and $\mu_0H_T \leq -2$ T, the magnetic hysteresis loop remains symmetric in both 6SL #1 and 8SL #1. This observation confirms the absence of the exchange bias effect in these two devices.

To understand the SL-dependent exchange bias effect in $MnBi_2Te_4$ devices, we conduct a numerical simulation based on the SL-resolved macro-spin model. The free energy is[47]

$$F = \sum_{i=1}^{N-1} J_{i,i+1}\boldsymbol{M}_i\cdot\boldsymbol{M}_{i+1} - \sum_{i=1}^{N}\left[\frac{\kappa_i}{2}(\boldsymbol{e}_i\cdot\boldsymbol{M}_i)^2 + \mu_0\boldsymbol{H}\cdot\boldsymbol{M}_i\right] \tag{1}$$

where $\boldsymbol{M}_i$ is the magnetic vector of the ith SL, $J_{i,i+1}$ is the AFM exchange interaction between the ith and $(i + 1)$th SLs, and $\mu_0\boldsymbol{H} = \mu_0H_z$ is the external magnetic field along the z-direction. Here, the key point is to allow the easy-axis direction $\boldsymbol{e}_i$ and its strength κ_i to be SL-specific, accounting for the difference between the outermost SLs and inner SLs (ref 48, Supporting Information). In our calculations, the bulk exchange interaction $J_b = 0.4$ meV and the bulk magnetic anisotropy is $\kappa_b = 0.1$ meV (refs 30, 46, and 47), while the surface exchange

https://doi.org/10.1021/acs.nanolett.4c01597
Nano Lett. 2024, 24, 8320−8326

interaction is J_s = 0.04 meV and the surface magnetic anisotropy is κ_s = 0.1 meV. We define $\delta\theta_s$ to characterize the easy axis direction of the surface SLs (i = 1 and i = N), specifically as the polar angle between the easy-axis direction $\boldsymbol{e}_i$ and the z-axis. In our calculations, we set $\delta\theta_s$ = 0.01 for both top and bottom surface SLs (Supporting Information). All of these parameters remain fixed in all of our devices with different layer numbers. By numerically minimizing the free energy, we obtained the stationary magnetic configuration. Parts a−c of Figure 4 show the magnetic evolution for 6 SL, 7 SL, and 8 SL $MnBi_2Te_4$ under opposite H_Ts. Under high magnetic training fields ($|\mu_0H_T| > |\mu_0H_S|$), the samples will enter a canted-AFM state with tilted magnetic moment angles. For the 7 SL $MnBi_2Te_4$, the magnetic hysteresis loop shifts to the opposite direction of H_T, resulting in a negative exchange bias effect such that $H_{cL} + H_{cR} > 0$ ($H_{cL} + H_{cR} < 0$) for $H_T < 0$ ($H_T > 0$). Specifically, for $H_T < 0$, $\mu_0H_{cL} = -0.66$ T and μ_0H_{cR} = +1.08 T, while, for $H_T > 0$, $\mu_0H_{cL} = -1.08$ T and μ_0H_{c+} = +0.66 T. The magnetic evolution obtained here agrees quantitatively with our experimental results (Figure 2c). In contrast, for both the 6 and 8 SL $MnBi_2Te_4$, the exchange bias effect is absent (Figure 4a−c), consistent with the experimental results in Figure 3c and d. We note that a step-like evolution of the magnetic configuration in both 6 SL and 8 SL $MnBi_2Te_4$ is not seen in our electrical transport results, but this observation is consistent with prior RMCD measurements on even SL $MnBi_2Te_4$ flakes.[30]

To gain a more intuitive understanding, we next employ an effective picture for $|\mu_0H| < |\mu_0H_s|$ and revisit the energy minimization from the perspective of the top SL (i = 1). The rationale behind this picture is that the magnetic configuration of the inner SLs remains unchanged for $|\mu_0H| < |\mu_0H_s|$; thus its contribution to the free energy in eq 1 is constant, allowing us to focus on the magnetic evolution of the top SL relative to the rest. A similar argument is applicable for the bottom SL ($i = N$) as well. Without losing generality, we assume that all magnetic moments rotate on the xz-plane and take M = 1 for simplicity. The reduced free energy for the top SL can then be expressed as

$$F_t = J_{1,2}\cos(\theta_1 - \theta_2) - \frac{\kappa_1}{2}\cos^2(\theta_1 - \delta\theta_s) - \mu_0 H\cos\theta_1 \quad (2)$$

where θ_1 and θ_2 describe the directions of the magnetic moments in the top SL and the second top SL and $\delta\theta_s$ characterizes the actual direction of the easy-axis anisotropy for the top SL (i = 1). By minimizing this free energy, we can obtain the magnetic evolution of the top surface SL for $|\mu_0H| < |\mu_0H_s|$. Both μ_0H_{cL} and μ_0H_{cR} occur, where the Zeeman energy compensates for the anisotropy. When $\theta_2 = 0$ (π), i.e., the magnetization in the second top SL points upward (downward), the magnetic hysteresis loop of the top SL (θ_1) shifts to the positive (negative) μ_0H direction (Figure 4d and e). Note that the magnetic evolution of the bottom SL (θ_N) exhibits the same behavior as it is described by the same free energy (Supporting Information).

For odd SL $MnBi_2Te_4$, magnetic moments in the second top and second bottom SLs are parallel ($\theta_2 = \theta_{N-1}$, Figure 4b), leading to the same magnetic evolution in the top SL and the bottom SL. Both centers of magnetic hysteresis loops corresponding to the top and bottom SLs shift in the same direction, leading to the appearance of the exchange bias effect. In contrast, for even SL $MnBi_2Te_4$, magnetic moments in the second top and second bottom SLs are antiparallel ($\theta_2 = \theta_{N-1} = \pi$, or reversely, Figure 4a−c). The magnetic hysteresis loops of the top and bottom SLs shift to opposite directions and thus cancel each other, rendering the absence of the exchange bias effect in even SL devices. We note that the strength of the exchange bias effect (i.e., $|\mu_0H_E|$) should remain constant for $|\mu_0H_T| > |\mu_0H_s|$. Our simulations confirm that the distinct magnetic properties of the surface and bulk SLs in $MnBi_2Te_4$ lead to the SL-dependent exchange bias effect.

To summarize, we observe an even−odd layer-dependent exchange bias effect in $MnBi_2Te_4$ Chern insulator devices. We find that the negative exchange bias effect in odd SL $MnBi_2Te_4$ devices is independent of the strength of the training magnetic field. The observation of the even−odd layer-dependent exchange bias effect demonstrates that the surface magnetic property plays a critical role in the formation of the magnetic hysteresis loop near zero magnetic field in $MnBi_2Te_4$ devices. Moreover, our findings provide new insights into the microscopic magnetic configuration in $MnBi_2Te_4$ thin flakes, which will advance the development of Chern-insulator-based electronic and spintronic devices with low power consumption.

ASSOCIATED CONTENT

Supporting Information

The Supporting Information is available free of charge at https://pubs.acs.org/doi/10.1021/acs.nanolett.4c01597.

Fabrication of $MnBi_2Te_4$ devices, electrical transport measurements, theoretical calculations, and more transport results of $MnBi_2Te_4$ devices with different thicknesses (PDF)

AUTHOR INFORMATION

Corresponding Authors

Cui-Zu Chang − *Department of Physics, The Pennsylvania State University, University Park, Pennsylvania 16802, United States;* orcid.org/0000-0003-3515-2955; Email: cxc955@psu.edu

Ran Cheng − *Department of Electrical and Computer Engineering, University of California, Riverside, California 92521, United States; Department of Physics and Astronomy, University of California, Riverside, California 92521, United States;* orcid.org/0000-0003-0166-2172; Email: ran.cheng@ucr.edu

Authors

Bo Chen − *Department of Physics, The Pennsylvania State University, University Park, Pennsylvania 16802, United States; National Laboratory of Solid State Microstructures, Collaborative Innovation Center of Advanced Microstructures, and School of Physics, Nanjing University, Nanjing 210093, China*

Xiaoda Liu − *Department of Physics, The Pennsylvania State University, University Park, Pennsylvania 16802, United States*

Yuhang Li − *School of Physics, Nankai University, Tianjin 300071, China; Department of Electrical and Computer Engineering, University of California, Riverside, California 92521, United States*

Han Tay − *Department of Physics, The Pennsylvania State University, University Park, Pennsylvania 16802, United States*

https://doi.org/10.1021/acs.nanolett.4c01597
Nano Lett. 2024, 24, 8320−8326

Takashi Taniguchi − *Research Center for Materials Nanoarchitectonics, National Institute for Materials Science, Tsukuba 305-0044, Japan;* orcid.org/0000-0002-1467-3105

Kenji Watanabe − *Research Center for Electronic and Optical Materials, National Institute for Materials Science, Tsukuba 305-0044, Japan;* orcid.org/0000-0003-3701-8119

Moses H. W. Chan − *Department of Physics, The Pennsylvania State University, University Park, Pennsylvania 16802, United States*

Jiaqiang Yan − *Materials Science and Technology Division, Oak Ridge National Laboratory, Oak Ridge, Tennessee 37831, United States;* orcid.org/0000-0001-6625-4706

Fengqi Song − *National Laboratory of Solid State Microstructures, Collaborative Innovation Center of Advanced Microstructures, and School of Physics, Nanjing University, Nanjing 210093, China;* orcid.org/0000-0001-6266-6551

Complete contact information is available at:
https://pubs.acs.org/10.1021/acs.nanolett.4c01597

Author Contributions

[$]B.C., X.L., Y.L.: These authors contributed equally. C.-Z.C. conceived and supervised the experiment. B.C., X.L., and H.T. fabricated all $MnBi_2Te_4$ devices and performed PPMS measurements. Y.L. and R.C. provided theoretical support. T.T. and K.W. provided *h*-BN crystals. J.Y. grew $MnBi_2Te_4$ crystals. B.C., X.L., and C.-Z.C. analyzed the data and wrote the manuscript with input from all authors.

Notes

The authors declare no competing financial interest.

■ ACKNOWLEDGMENTS

We thank J. Cai, Y. Cui, C. -X. Liu, R. Mei, Y. Zhang, and X. Xu for helpful discussions. This work is primarily supported by the ONR Award (N000142412133), including device fabrication and sample characterization. The PPMS measurements are partially supported by the NSF grant (DMR-2241327) and ARO grant (W911NF2210159). C.-Z.C. acknowledges the support from the Gordon and Betty Moore Foundation's EPiQS Initiative (GBMF9063 to C.-Z.C.). K.W. and T.T. acknowledge support from the JSPS KAKENHI (20H00354 and 23H02052) and World Premier International Research Center Initiative (WPI), MEXT, Japan. Work done at UCR was supported by the AFOSR Grant (FA9550-19-1-0307). Work done at ORNL was supported by the US Department of Energy, Office of Science, Basic Energy Sciences, Materials Sciences and Engineering Division.

■ REFERENCES

(1) Qi, X. L.; Hughes, T. L.; Zhang, S. C. Topological Field Theory of Time-Reversal Invariant Insulators. *Phys. Rev. B* **2008**, *78*, No. 195424.

(2) Liu, C. X.; Qi, X. L.; Dai, X.; Fang, Z.; Zhang, S. C. Quantum anomalous Hall effect in $Hg_{1-y}Mn_yTe$ quantum wells. *Phys. Rev. Lett.* **2008**, *101*, No. 146802.

(3) Yu, R.; Zhang, W.; Zhang, H. J.; Zhang, S. C.; Dai, X.; Fang, Z. Quantized Anomalous Hall Effect in Magnetic Topological Insulators. *Science* **2010**, *329*, 61−64.

(4) Chang, C. Z.; Zhang, J. S.; Feng, X.; Shen, J.; Zhang, Z. C.; Guo, M. H.; Li, K.; Ou, Y. B.; Wei, P.; Wang, L. L.; Ji, Z. Q.; Feng, Y.; Ji, S. H.; Chen, X.; Jia, J. F.; Dai, X.; Fang, Z.; Zhang, S. C.; He, K.; Wang, Y. Y.; Lu, L.; Ma, X. C.; Xue, Q. K. Experimental Observation of the Quantum Anomalous Hall Effect in a Magnetic Topological Insulator. *Science* **2013**, *340*, 167−170.

(5) Chang, C. Z.; Zhang, J. S.; Liu, M. H.; Zhang, Z. C.; Feng, X.; Li, K.; Wang, L. L.; Chen, X.; Dai, X.; Fang, Z.; Qi, X. L.; Zhang, S. C.; Wang, Y. Y.; He, K.; Ma, X. C.; Xue, Q. K. Thin Films of Magnetically Doped Topological Insulator with Carrier-Independent Long-Range Ferromagnetic Order. *Adv. Mater.* **2013**, *25*, 1065−1070.

(6) Chang, C. Z.; Wei, P.; Moodera, J. S. Breaking Time Reversal Symmetry in Topological Insulators. *MRS Bull.* **2014**, *39*, 867−872.

(7) Tokura, Y.; Yasuda, K.; Tsukazaki, A. Magnetic topological insulators. *Nat. Rev. Phys.* **2019**, *1*, 126−143.

(8) Bernevig, B. A.; Felser, C.; Beidenkopf, H. Progress and prospects in magnetic topological materials. *Nature* **2022**, *603*, 41−51.

(9) Chang, C.-Z.; Liu, C.-X.; MacDonald, A. H. Colloquium: Quantum anomalous Hall effect. *Rev. Mod. Phys.* **2023**, *95*, No. 011002.

(10) Kou, X. F.; Guo, S. T.; Fan, Y. B.; Pan, L.; Lang, M. R.; Jiang, Y.; Shao, Q. M.; Nie, T. X.; Murata, K.; Tang, J. S.; Wang, Y.; He, L.; Lee, T. K.; Lee, W. L.; Wang, K. L. Scale-Invariant Quantum Anomalous Hall Effect in Magnetic Topological Insulators beyond the Two-Dimensional Limit. *Phys. Rev. Lett.* **2014**, *113*, No. 137201.

(11) Checkelsky, J. G.; Yoshimi, R.; Tsukazaki, A.; Takahashi, K. S.; Kozuka, Y.; Falson, J.; Kawasaki, M.; Tokura, Y. Trajectory of the Anomalous Hall Effect towards the Quantized State in a Ferromagnetic Topological Insulator. *Nat. Phys.* **2014**, *10*, 731−736.

(12) Chang, C. Z.; Zhao, W. W.; Kim, D. Y.; Zhang, H. J.; Assaf, B. A.; Heiman, D.; Zhang, S. C.; Liu, C. X.; Chan, M. H. W.; Moodera, J. S. High-Precision Realization of Robust Quantum Anomalous Hall State in a Hard Ferromagnetic Topological Insulator. *Nat. Mater.* **2015**, *14*, 473−477.

(13) Deng, Y.; Yu, Y.; Shi, M. Z.; Guo, Z.; Xu, Z.; Wang, J.; Chen, X. H.; Zhang, Y. Quantum anomalous Hall effect in intrinsic magnetic topological insulator $MnBi_2Te_4$. *Science* **2020**, *367*, 895−900.

(14) Xiao, D.; Jiang, J.; Shin, J. H.; Wang, W. B.; Wang, F.; Zhao, Y. F.; Liu, C. X.; Wu, W. D.; Chan, M. H. W.; Samarth, N.; Chang, C. Z. Realization of the Axion Insulator State in Quantum Anomalous Hall Sandwich Heterostructures. *Phys. Rev. Lett.* **2018**, *120*, No. 056801.

(15) Mogi, M.; Kawamura, M.; Tsukazaki, A.; Yoshimi, R.; Takahashi, K. S.; Kawasaki, M.; Tokura, Y. Tailoring Tricolor Structure of Magnetic Topological Insulator for Robust Axion Insulator. *Sci. Adv.* **2017**, *3*, No. eaao1669.

(16) Zhuo, D.; Yan, Z. J.; Sun, Z. T.; Zhou, L. J.; Zhao, Y. F.; Zhang, R.; Mei, R.; Yi, H.; Wang, K.; Chan, M. H. W.; Liu, C. X.; Law, K. T.; Chang, C. Z. Axion insulator state in hundred-nanometer-thick magnetic topological insulator sandwich heterostructures. *Nat. Commun.* **2023**, *14*, 7596.

(17) Liu, D. F.; Liang, A. J.; Liu, E. K.; Xu, Q. N.; Li, Y. W.; Chen, C.; Pei, D.; Shi, W. J.; Mo, S. K.; Dudin, P.; Kim, T.; Cacho, C.; Li, G.; Sun, Y.; Yang, L. X.; Liu, Z. K.; Parkin, S. S. P.; Felser, C.; Chen, Y. L. Magnetic Weyl semimetal phase in a Kagome crystal. *Science* **2019**, *365*, 1282−1285.

(18) Morali, N.; Batabyal, R.; Nag, P. K.; Liu, E. K.; Xu, Q. A.; Sun, Y.; Yan, B. H.; Felser, C.; Avraham, N.; Beidenkopf, H. Fermi-arc diversity on surface terminations of the magnetic Weyl semimetal $Co_3Sn_2S_2$. *Science* **2019**, *365*, 1286−1291.

(19) Schindler, F.; Cook, A. M.; Vergniory, M. G.; Wang, Z. J.; Parkin, S. S. P.; Bernevig, B. A.; Neupert, T. Higher-order topological insulators. *Sci. Adv.* **2018**, *4*, No. eaat0346.

(20) Zhang, R. X.; Cole, W. S.; Wu, X. X.; Das Sarma, S. Higher-Order Topology and Nodal Topological Superconductivity in Fe(Se,Te) Heterostructures. *Phys. Rev. Lett.* **2019**, *123*, No. 167001.

(21) Chang, C. Z. Marriage of topology and magnetism. *Nat. Mater.* **2020**, *19*, 484−485.

(22) Li, J. H.; Li, Y.; Du, S. Q.; Wang, Z.; Gu, B. L.; Zhang, S. C.; He, K.; Duan, W. H.; Xu, Y. Intrinsic Magnetic Topological Insulators in van der Waals Layered $MnBi_2Te_4$-Family Materials. *Sci. Adv.* **2019**, *5*, No. eaaw5685.

(23) Zhang, D. Q.; Shi, M. J.; Zhu, T. S.; Xing, D. Y.; Zhang, H. J.; Wang, J. Topological Axion States in the Magnetic Insulator $MnBi_2Te_4$ with the Quantized Magnetoelectric Effect. *Phys. Rev. Lett.* **2019**, *122*, No. 206401.

(24) Otrokov, M. M.; Klimovskikh, I. I.; Bentmann, H.; Estyunin, D.; Zeugner, A.; Aliev, Z. S.; Gass, S.; Wolter, A. U. B.; Koroleva, A. V.; Shikin, A. M.; Blanco-Rey, M.; Hoffmann, M.; Rusinov, I. P.; Vyazovskaya, A. Y.; Eremeev, S. V.; Koroteev, Y. M.; Kuznetsov, V. M.; Freyse, F.; Sanchez-Barriga, J.; Amiraslanov, I. R.; Babanly, M. B.; Mamedov, N. T.; Abdullayev, N. A.; Zverev, V. N.; Alfonsov, A.; Kataev, V.; Buchner, B.; Schwier, E. F.; Kumar, S.; Kimura, A.; Petaccia, L.; Di Santo, G.; Vidal, R. C.; Schatz, S.; Kissner, K.; Unzelmann, M.; Min, C. H.; Moser, S.; Peixoto, T. R. F.; Reinert, F.; Ernst, A.; Echenique, P. M.; Isaeva, A.; Chulkov, E. V. Prediction and observation of an antiferromagnetic topological insulator. *Nature* **2019**, *576*, 416−422.

(25) Gong, Y.; Guo, J.; Li, J.; Zhu, K.; Liao, M.; Liu, X.; Zhang, Q.; Gu, L.; Tang, L.; Feng, X.; Zhang, D.; Li, W.; Song, C.; Wang, L.; Yu, P.; Chen, X.; Wang, Y.; Yao, H.; Duan, W.; Xu, Y.; Zhang, S.-C.; Ma, X.; Xue, Q.-K.; He, K. Experimental Realization of an Intrinsic Magnetic Topological Insulator. *Chin. Phys. Lett.* **2019**, *36*, No. 076801.

(26) Yan, J. Q.; Zhang, Q.; Heitmann, T.; Huang, Z. L.; Chen, K. Y.; Cheng, J. G.; Wu, W. D.; Vaknin, D.; Sales, B. C.; McQueeney, R. J. Crystal growth and magnetic structure of $MnBi_2Te_4$. *Phys. Rev. Mater.* **2019**, *3*, No. 064202.

(27) Otrokov, M. M.; Rusinov, I. P.; Blanco-Rey, M.; Hoffmann, M.; Vyazovskaya, A. Y.; Eremeev, S. V.; Ernst, A.; Echenique, P. M.; Arnau, A.; Chulkov, E. V. Unique Thickness-Dependent Properties of the van der Waals Interlayer Antiferromagnet $MnBi_2Te_4$ Films. *Phys. Rev. Lett.* **2019**, *122*, No. 107202.

(28) Liu, C.; Wang, Y. C.; Li, H.; Wu, Y.; Li, Y. X.; Li, J. H.; He, K.; Xu, Y.; Zhang, J. S.; Wang, Y. Y. Robust axion insulator and Chern insulator phases in a two-dimensional antiferromagnetic topological insulator. *Nat. Mater.* **2020**, *19*, 522−527.

(29) Ge, J.; Liu, Y.; Li, J.; Li, H.; Luo, T.; Wu, Y.; Xu, Y.; Wang, J. High-Chern-Number and High-Temperature Quantum Hall Effect without Landau Levels. *Natl. Sci. Rev.* **2020**, *7*, 1280−1287.

(30) Ovchinnikov, D.; Huang, X.; Lin, Z.; Fei, Z.; Cai, J.; Song, T.; He, M.; Jiang, Q.; Wang, C.; Li, H.; Wang, Y.; Wu, Y.; Xiao, D.; Chu, J. H.; Yan, J.; Chang, C. Z.; Cui, Y. T.; Xu, X. Intertwined Topological and Magnetic Orders in Atomically Thin Chern Insulator $MnBi_2Te_4$. *Nano Lett.* **2021**, *21*, 2544−2550.

(31) Cai, J. Q.; Ovchinnikov, D.; Fei, Z. Y.; He, M. H.; Song, T. C.; Lin, Z.; Wang, C.; Cobden, D.; Chu, J. H.; Cui, Y. T.; Chang, C. Z.; Xiao, D.; Yan, J. Q.; Xu, X. D. Electric control of a canted-antiferromagnetic Chern insulator. *Nat. Commun.* **2022**, *13*, 1668.

(32) Ovchinnikov, D.; Cai, J. Q.; Lin, Z.; Fei, Z. Y.; Liu, Z. Y.; Cui, Y. T.; Cobden, D. H.; Chu, J. H.; Chang, C. Z.; Xiao, D.; Yan, J. Q.; Xu, X. D. Topological current divider in a Chern insulator junction. *Nat. Commun.* **2022**, *13*, 5967.

(33) Gao, A. Y.; Liu, Y. F.; Hu, C. W.; Qiu, J. X.; Tzschaschel, C.; Ghosh, B.; Ho, S. C.; Berube, D.; Chen, R.; Sun, H. P.; Zhang, Z. W.; Zhang, X. Y.; Wang, Y. X.; Wang, N. Z.; Huang, Z. M.; Felser, C.; Agarwal, A.; Ding, T.; Tien, H. J.; Akey, A.; Gardener, J.; Singh, B.; Watanabe, K.; Taniguchi, T.; Burch, K. S.; Bell, D. C.; Zhou, B. B.; Gao, W. B.; Lu, H. Z.; Bansil, A.; Lin, H.; Chang, T. R.; Fu, L.; Ma, Q.; Ni, N.; Xu, S. Y. Layer Hall effect in a 2D topological axion antiferromagnet. *Nature* **2021**, *595*, 521−525.

(34) Ying, Z.; Zhang, S.; Chen, B.; Jia, B.; Fei, F. C.; Zhang, M. H.; Zhang, H. J.; Wang, X. F.; Song, F. Q. Experimental evidence for dissipationless transport of the chiral edge state of the high-field Chern insulator in $MnBi_2Te_4$ nanodevices. *Phys. Rev. B* **2022**, *105*, No. 085412.

(35) Nogues, J.; Schuller, I. K. Exchange Bias. *J. Magn. Magn. Mater.* **1999**, *192*, 203−232.

(36) Kiwi, M. Exchange bias theory. *J. Magn. Magn. Mater.* **2001**, *234*, 584−595.

(37) Nogues, J.; Lederman, D.; Moran, T. J.; Schuller, I. K. Positive Exchange Bias in FeF_2-Fe Bilayers. *Phys. Rev. Lett.* **1996**, *76*, 4624−4627.

(38) Nogues, J.; Leighton, C.; Schuller, I. K. Correlation between Antiferromagnetic Interface Coupling and Positive Exchange Bias. *Phys. Rev. B* **2000**, *61*, 1315−1317.

(39) Yang, D. Z.; Du, J.; Sun, L.; Wu, X. S.; Zhang, X. X.; Zhou, S. M. Positive Exchange Biasing In GdFe/NiCoO Bilayers with Antiferromagnetic Coupling. *Phys. Rev. B* **2005**, *71*, No. 144417.

(40) Wang, F.; Xiao, D.; Yuan, W.; Jiang, J.; Zhao, Y.-F.; Zhang, L.; Yao, Y.; Liu, W.; Zhang, Z.; Liu, C.; Shi, J.; Han, W.; Chan, M. H. W.; Samarth, N.; Chang, C.-Z. Observation of Interfacial Antiferromagnetic Coupling between Magnetic Topological Insulator and Antiferromagnetic Insulator. *Nano Lett.* **2019**, *19*, 2945−2952.

(41) Fu, H. X.; Liu, C. X.; Yan, B. H. Exchange bias and quantum anomalous Hall effect in the $MnBi_2Te_4/CrI_3$ heterostructure. *Sci. Adv.* **2020**, *6*, No. eaaz0948.

(42) Ying, Z.; Chen, B.; Li, C. F.; Wei, B. Y.; Dai, Z.; Guo, F. Y.; Pan, D. F.; Zhang, H. J.; Wu, D.; Wang, X. F.; Zhang, S.; Fei, F. C.; Song, F. Q. Large Exchange Bias Effect and Coverage-Dependent Interfacial Coupling in $CrI_3/MnBi_2Te_4$ van der Waals Heterostructures. *Nano Lett.* **2023**, *23*, 765−771.

(43) Fang, J. Z.; Cui, H. N.; Wang, S.; Lu, J. D.; Zhu, G. Y.; Liu, X. J.; Qin, M. S.; Wang, J. K.; Wu, Z. N.; Wu, Y. F.; Wang, S. G.; Zhang, Z. S.; Wei, Z. M.; Zhang, J. X.; Lin, B. C.; Liao, Z. M.; Yu, D. P. Exchange bias in the van der Waals heterostructure $MnBi_2Te_4/Cr_2Ge_2Te_6$. *Phys. Rev. B* **2023**, *107*, No. L041107.

(44) Zang, Z. H.; Xi, M.; Tian, S. J.; Guzman, R.; Wang, T. T.; Zhou, W.; Lei, H. C.; Huang, Y.; Ye, Y. Exchange Bias Effects in Ferromagnetic $MnSb_2Te_4$ down to a Monolayer. *ACS Appl. Electron. Mater.* **2022**, *4*, 3256.

(45) Xu, X. L.; Yang, S. Q.; Wang, H.; Guzman, R.; Gao, Y. C.; Zhu, Y. Z.; Peng, Y. X.; Zang, Z. H.; Xi, M.; Tian, S. J.; Li, Y. P.; Lei, H. C.; Luo, Z. C.; Yang, J. B.; Wang, Y. L.; Xia, T. L.; Zhou, W.; Huang, Y.; Ye, Y. Ferromagnetic-antiferromagnetic coexisting ground state and exchange bias effects in $MnBi_4Te_7$ and $MnBi_6Te_{10}$. *Nat. Commun.* **2022**, *13*, 7646.

(46) Yang, S.; Xu, X.; Zhu, Y.; Niu, R.; Xu, C.; Peng, Y.; Cheng, X.; Jia, X.; Huang, Y.; Xu, X.; Lu, J.; Ye, Y. Odd-Even Layer-Number Effect and Layer-Dependent Magnetic Phase Diagrams in $MnBi_2Te_4$. *Phys. Rev. X* **2021**, *11*, No. 011003.

(47) Li, Y. H.; Cheng, R. Identifying axion insulator by quantized magnetoelectric effect in antiferromagnetic $MnBi_2Te_4$ tunnel junction. *Phys. Rev. Research* **2022**, *4*, No. L022067.

(48) Tan, H. X.; Yan, B. H. Distinct Magnetic Gaps between Antiferromagnetic and Ferromagnetic Orders Driven by Surface Defects in the Topological Magnet $MnBi_2Te_4$. *Phys. Rev. Lett.* **2023**, *130*, No. 126702.